Atmos. Chem. Phys. Discuss., 10, 13519–13555, 2010
www.atmos-chem-phys-discuss.net/10/13519/2010/
doi:10.5194/acpd-10-13519-2010

Atmospheric Chemistry and Physics Discussions

History of atmospheric SF_6 from 1973 to 2008

M. Rigby[1], J. Mühle[2], B. R. Miller[3], R. G. Prinn[1], P. B. Krummel[4], L. P. Steele[4], P. J. Fraser[4], P. K. Salameh[2], C. M. Harth[2], R. F. Weiss[2], B. R. Greally[5], S. O'Doherty[5], P. G. Simmonds[5], M. K. Vollmer[6], S. Reimann[6], J. Kim[7], K. R. Kim[7], H. J. Wang[8], E. J. Dlugokencky[9], G. S. Dutton[9], B. D. Hall[9], and J. W. Elkins[9]

[1]Center for Global Change Science, Massachusetts Institute of Technology, 77 Massachusetts Ave., Cambridge, 02139 MA, USA
[2]Scripps Institution of Oceanography, University of California at San Diego, La Jolla, CA, USA
[3]Cooperative Institute for Research in Environmental Sciences, University of Colorado, Boulder, CO, USA
[4]Centre for Australian Weather and Climate Research, CSIRO Marine and Atmospheric Research, Aspendale, Victoria, Australia
[5]School of Chemistry, University of Bristol, Bristol, UK
[6]Empa, Swiss Federal Laboratories for Materials Testing and Research, Switzerland

[7]School of Earth and Environmental Sciences, Seoul National University, South Korea
[8]School of Earth and Atmospheric Sciences, Georgia Institute of Technology, Atlanta, GA, USA
[9]Earth System Research Laboratory, NOAA, Boulder, CO, USA

Received: 7 May 2010 – Accepted: 16 May 2010 – Published: 28 May 2010

Correspondence to: M. Rigby (mrigby@mit.edu)

Published by Copernicus Publications on behalf of the European Geosciences Union.

Abstract

We present atmospheric sulfur hexafluoride (SF_6) mole fractions and emissions estimates from the 1970s to 2008. Measurements were made of archived air samples starting from 1973 in the Northern Hemisphere and from 1978 in the Southern Hemisphere, using the Advanced Global Atmospheric Gases Experiment (AGAGE) gas chromatographic–mass spectrometric (GC-MS) systems. These measurements were combined with modern high-frequency GC-MS and GC-electron capture detection (ECD) data from AGAGE monitoring sites, to produce a unique air history of this potent greenhouse gas. Atmospheric mole fractions were found to have increased by more than an order of magnitude between 1973 and 2008. The 2008 growth rate was found to be the highest recorded, at 0.29 ± 0.02 pmol mol^{-1} yr^{-1}. A three-dimensional chemical transport model and a minimum variance Bayesian inverse method was used to estimate annual emission rates using the measurements. Consistent with the mole fraction growth rate maximum, global emissions during 2008 were also found to be highest in the 1973–2008 period, reaching 7.5 ± 0.4 Gg yr^{-1} and surpassing the previous maximum in 1995. The 2008 values follow an increase in emissions of 50 ± 25% since 2000. A second global inversion which also incorporated National Oceanic and Atmospheric Administration (NOAA) flask measurements and in situ monitoring site data was found to agree well with the emissions derived using AGAGE measurements alone. By estimating continent-scale emissions using all available AGAGE and NOAA surface measurements covering the period 2004–2008, we find that it is likely that much of the global emissions rise during this five-year period originated primarily from Asian countries that do not report emissions to the United Nations Framework Convention on Climate Change (UNFCCC). We also find it likely that SF_6 emissions reported to the UNFCCC were underestimated between at least 2004 and 2007.

ACPD
10, 13519–13555, 2010

1 Introduction

With a global warming potential of around 22 800 over a 100-year time horizon, sulfur hexafluoride (SF_6) is the most potent greenhouse gas regulated under the Kyoto Protocol (by mass, Forster et al., 2007; Rinsland et al., 1990). The concentration of SF_6 in the atmosphere is currently relatively low, leading to a contribution to the total anthropogenic radiative forcing of the order of 0.1%. However, its long lifetime of ~3200 years means that levels will only increase over human timescales (Ravishankara et al., 1993). Given these considerations, it is important that estimates of emissions of this compound are well constrained using both "bottom-up" and "top-down" methods so that emissions reduction strategies can be properly designed and evaluated.

Sulfur hexafluoride is primarily used as a dielectric and insulator in high voltage electrical equipment, from which it is released to the atmosphere through leakage and during repair (Niemeyer and Chu, 1992). It is also released from a variety of more minor sources including the aluminum and magnesium industries (Fraser et al., 2004). Natural sources of SF_6 are very small (Deeds et al., 2008), leading to a very low estimated pre-industrial concentration, derived from firn air measurements, of $\sim 6 \times 10^{-3}$ pmol mol^{-1} (Vollmer and Weiss, 2002), compared to more than 6 pmol mol^{-1} in 2008. Its overwhelmingly anthropogenic origin means that SF_6 emissions are very highly weighted to the Northern Hemisphere (NH), with previous studies estimating a 94% NH contribution to the global total (Maiss et al., 1996).

Previous work has examined the concentration and growth of atmospheric SF_6 during various intervals, using measurements made with different instruments. Maiss and Levin (1994) and Maiss et al. (1996) reported an increase in the global atmospheric burden throughout the 1980s and early 1990s using GC-ECD measurements of air samples taken at a number of background sites. They found that mole fractions increased almost quadratically with time during this period, implying a near-linear rise in emissions. Geller et al. (1997) confirmed this finding using GC-ECD measurements of air samples collected at the NOAA Earth System Research Laboratory (ESRL)

ACPD
10, 13519–13555, 2010

sites. Using a two-box model of the troposphere they derived a global emission rate of $5.9 \pm 0.2\,\mathrm{Ggyr}^{-1}$ for 1996. Fraser et al. (2004) reported high-frequency in situ GC-ECD measurements at Cape Grim, Tasmania starting in 2001. They deduced that global emissions had remained relatively constant from 1995 to 2003 within $\pm 10\%$. Most recently, Levin et al. (2010) reported Southern Hemisphere (SH) measurements beginning in 1978 and NH measurements beginning in 1981, showing a renewed increase in the rise rate from 1997 to 2008. They inferred SF_6 emissions by estimating the atmospheric burden and taking its derivative with respect to time. A two-dimensional atmospheric box model was then used to simulate atmospheric mole fractions based on these emissions, which were compared to the measurements to check that the derived emissions were reasonable. Some studies have derived regional emissions for SF_6. Emissions for Northern China were investigated using a Lagrangian model, and GC-ECD measurements at the Shangdianzi station by Vollmer et al. (2009). Airborne SF_6 measurements were also used to determine North American emissions in 2003 (Hurst et al., 2006).

Given that it is highly chemically inert and relatively easy to measure, many geophysical applications have been found for SF_6. These include validation of chemical transport model advection schemes (Gloor et al., 2007; Peters et al., 2004), determination of the age of stratospheric air (e.g. Hall and Waugh, 1997), investigation of the relative importance of atmospheric transport processes (Patra et al., 2009) and groundwater dating (e.g. Bunsenberg and Plummer , 2000). Each of these applications rely on an accurate knowledge of the atmospheric history of SF_6. Small amounts of SF_6 are also intentionally released to the atmosphere for a variety of purposes, including the tracking of urban air movements and the detection of leaks in reticulated gas systems.

In this paper we use a three-dimensional chemical transport model to derive annual hemispheric emission rates from 1973–2008 using new measurements of archived air samples collected at Cape Grim, Tasmania, and NH archived air samples mostly collected at Trinidad Head, California, along with modern ambient measurements from the Advanced Global Atmospheric Gases Experiment (AGAGE, Prinn et al., 2000).

ACPD
10, 13519–13555, 2010

We then use additional data from the NOAA-ESRL ask and in situ networks to derive annual hemispheric and then regional-scale emissions using data from both networks. This work improves on the approach of Levin et al. (2010) by extending the NH record 8 years further back, by using a three-dimensional chemical transport model to derive emissions with an inverse approach that considers measurement error and allows for the incorporation of useful prior information, and by attempting to resolve regional sources.

The derived emissions are compared to the Emissions Database for Global Atmospheric Research (EDGAR v4, European Comission, 2009) and reports to the United Nations Framework Convention on Climate Change (UNFCCC, 2010). The 39 countries that report emissions to the UNFCCC are Australia, Austria, Belarus, Belgium, Bulgaria, Canada, Croatia, Czech Republic, Denmark, Estonia, Finland, France, Germany, Greece, Hungary, Iceland, Ireland, Italy, Japan, Latvia, Liechtenstein, Lithuania, Luxembourg, Monaco, Netherlands, New Zealand, Norway, Poland, Portugal, Romania, Russia, Slovakia, Slovenia, Spain, Sweden, Switzerland, Turkey, UK and the USA.

2 Archived and ambient measurements

2.1 AGAGE measurements

AGAGE has been making high-frequency measurements of SF_6 at Cape Grim, Tasmania, using a GC-ECD system since 2001 (Fraser et al., 2004). From 2003, AGAGE stations also began measuring this compound with GC-MS "Medusa" systems (Miller et al., 2008).

To define the growth in the global background mole fraction, we used data from five AGAGE stations in the first part of this work: Cape Grim, Tasmania (since 2001), Trinidad Head, California (since 2005), Mace Head, Ireland (since 2003), Ragged Point, Barbados (since 2005) and Cape Matatula, American Samoa (since 2006). Table 1 shows the location of these background AGAGE sites. Additional ambient AGAGE

ACPD
10, 13519–13555, 2010

measurements from Gosan, Korea (since 2007) and Jungfraujoch, Switzerland (since 2008) were also used for regional emissions estimation in the second part of our analysis. The Cape Grim GC-ECD SF_6 measurements were discontinued in 2009.

To extend this time series back further than 2001, we report new AGAGE GC-MS Medusa measurements of samples from the Cape Grim Air Archive (CGAA) and a collection of Northern Hemisphere (NH) archived air samples. The CGAA consists primarily of whole air compressed by cryogenic trapping and archived into 35L stainless steel cylinders, with most of the condensed water being expelled after trapping (for details, see Langenfelds et al., 1996). 64 samples of the CGAA filled between 1978 and 2006 were measured at the Commonwealth Scientific and Industrial Research Organisation (CSIRO) Division of Marine and Atmospheric Research (CMAR, Aspendale, Australia). Six additional SH samples filled between 1995 and 2004 were measured at the Scripps Institution of Oceanography (SIO, La Jolla, California) and were found to be in excellent agreement with the SH samples with similar fill dates measured at CSIRO (mole fractions differed by $\Delta\chi$=0.001–0.05 pmol mol^{-1} for sampling time differences (Δt) of 3–33 days). 124 NH samples filled between 1973 and 2008 were measured at SIO. Four out of five additional NH samples filled between 1980 and 1999 were measured at CSIRO and were in excellent agreement with the NH samples with similar fill dates measured at SIO ($\Delta\chi$=0.003–0.05 pmol mol^{-1}, Δt=0–12 days). The fifth NH sample measured at CSIRO had a unique fill date (Δt=194 days to other tanks). These tests show that measurements at the two sites are in agreement, at least for mixing ratios in the range 0.9–5.1 pmol mol^{-1}. The 129 NH samples originate mostly from Trinidad Head, California and to a smaller extent from La Jolla, California (laboratories of R. F. Weiss, C. D. Keeling, and R. F. Keeling at Scripps Institution of Oceanography), Cape Meares, Oregon (NOAA-ESRL, Norwegian Institute for Air Research (NILU), and CSIRO, originally collected by R. A. Rasmussen and the Oregon Graduate Institute), Niwot Ridge, Colorado (NOAA-ESRL and NILU), and Barrow, Alaska (University of California, Berkeley). They were filled during periods when the sites intercepted background air, but with various filling techniques and for different

ACPD
10, 13519–13555, 2010

purposes. 29 NH samples had to be rejected as outliers with mostly higher mixing ratios for reasons such as initial retention of analytes on drying agents used during the filling followed by breakthrough, or sampling of polluted air, leaving 100 (81%) NH samples. None of the 70 (64 at CSIRO and 6 at SIO) SH samples had to be rejected, which is consistent with the strict procedures adopted for the collection of the CGAA samples (Langenfelds et al., 1996).

The long-term stability of SF_6 in the early CGAA samples has been evaluated empirically. Sub-samples of the CGAA were prepared at CMAR, Aspendale, and sent to the University of Heidelberg for analysis of SF_6 by GC-ECD in 1995 (see Maiss et al., 1996). Small corrections to the originally reported SF_6 mixing ratios were applied recently, after a careful reassessment of the non-linear response of the ECD (Levin et al., 2010). The Medusa GC-MS measurements of the CGAA samples were carried out in 2007 at CMAR, Aspendale, without the need to prepare explicit sub-samples (each CGAA cylinder was sampled directly, via a suitable pressure-reducing regulator). Comparison of both sets of measurements (made 12 years apart) show excellent agreement in the SF_6 trend, for CGAA samples collected in the period 1978–1994 (see supplementary material, http://www.atmos-chem-phys-discuss.net/10/13519/2010/acpd-10-13519-2010-supplement.zip). A small average offset of ~1.5% between the two sets of measurements is consistent with a difference of this magnitude between the two independently prepared SF_6 calibration scales. These results strongly support the contention that SF_6 has stored faithfully in the CGAA cylinders.

All AGAGE in situ and archived measurements are presented on the SIO–2005 scale as dry gas mole fractions in pmol mol^{-1}. Details of the calibration chain from SIO to each station are reported in Miller et al. (2008). The estimated accuracy of the calibration scale is 1–2%. The typical repeatability of reference gas measurements is ~0.05 pmol mol^{-1}, which was used as an estimate of the repeatability of each in situ measurement. Typical repeatability for archived air samples was ~0.02 pmol mol^{-1}, with 3–4 replicates for most older samples and 10–12 replicates for more recent samples.

ACPD
10, 13519–13555, 2010

Any non-linearity of the response of the Medusa GC-MS and any potential for system blank contamination in the analysis of the CGAA samples was experimentally determined to be negligible over the mole fraction range of the CGAA.

Figure 1 shows the SF_6 mole fractions from the CGAA and NH archive from 1973–2008. From 2001, monthly mole fractions from the Cape Grim GC-ECD are presented and starting around 2004 the Cape Grim and Trinidad Head AGAGE Medusa measurements are shown, following removal of local pollution events using the statistical filtering algorithm described in Prinn et al. (2000).

The measurements show that the SF_6 loading of the atmosphere has increased by more than a factor of 10 between 1973 and 2008. Close examination of the data indicates a steady acceleration of the mole fraction growth rate throughout the 1970s and 1980s, indicating a gradual rise in emission rate. This approximately quadratic increase with respect to time was previously noted by Maiss et al. (1996). The growth rate was seen to stabilize during the 1990s before accelerating again from around 2000, reaching $0.29 \pm 0.02\,\mathrm{pmol\,mol^{-1}\,yr^{-1}}$ in 2008 (lower panel, Fig. 1). This recent acceleration in growth was previously noted by Levin et al. (2010) and Elkins and Dutton (2009).

2.2 NOAA measurements

SF_6 data are from surface air samples collected as part of the NOAA Global Cooperative Air Sampling Network. Surface samples are collected in duplicate, approximately weekly, from a globally distributed network of background air sampling sites (Dlugokencky et al., 1994). Daily samples are collected at tall tower sites using flask and compressor packages built into suitcases for portability. The flask package contains 12 borosilicate glass flasks and a microprocessor to control flask valves. Flasks are cylindrical in shape, ~1 L volume, and have glass-piston, Teflon-O-ring sealed stopcocks on each end. Materials used in these flasks are identical to those used in the surface network. Custom-built actuators, controlled by the microprocessor, are used to open and close stopcocks. The compressor package contains two compressors connected in series. During sampling, flask and compressor packages are connected by cables

ACPD
10, 13519–13555, 2010

to transfer power and instructions from the microprocessor, and tubing to get air from the compressors to the flasks. For each sample, 10 L of ambient air is flushed through a flask, then it is pressurized to 0.28 MPa. The entire flask package is returned to Boulder for trace gas analysis, while the compressor package remains at the sampling site.

SF_6 dry-air mole fractions (pmol mol^{-1}) are determined at NOAA in Boulder, Colorado, USA by GC-ECD (for details, see Geller et al. (1997)). The ECD response to SF_6 is calibrated against the NOAA 2006 (gravimetrically-prepared) standard scale. Each aliquot of sample is bracketed by aliquots of natural air from a reference cylinder; repeatability of the analytical system is 0.04 pmol mol^{-1}, determined as one standard deviation of multiple measurements of air from a cylinder containing natural air. In addition to SF_6, samples are also analyzed for CH_4, CO_2, CO, H_2, N_2O, and $\delta^{13}C$ and $\delta^{18}O$ in CO_2.

Six NOAA field sites (SPO, SMO, MLO, BRW, NWR and SUM, see Table 1) are equipped with GCs that sample air from a 10 m tower once an hour. Each in situ GC is fitted with four electron capture detectors and packed or capillary columns tuned to measure a variety of trace gases including SF_6. To separate SF_6, two 1.59 mm outer-diameter packed columns of Porapak Q are used (2 m pre-column and 3 m main column) and are thermally controlled at 60°C. The air samples are compared to two on-site calibrated reference tanks with values assigned on the NOAA-2006 SF_6 scale that are sampled once every two hours. SF_6 estimated repeatability ranges from 0.03 to 0.05 pmol mol^{-1} at each in situ station.

2.3 Measurement intercomparison

Coincident AGAGE GC-ECD and GC-MS Medusa high-frequency measurements made at Cape Grim were found to compare very well with each other, with a mean bias of approximately 0.01 pmol mol^{-1}, and a standard deviation of 0.07 pmol mol^{-1}. Coincident AGAGE archive and high-frequency GC-MS Medusa measurements at Cape

ACPD
10, 13519–13555, 2010

Grim and at Trinidad Head/Mace Head also agree well with each other.

AGAGE measurements are regularly compared with the NOAA-ESRL in situ and flask networks where coincident measurements exist (NOAA flask samples are collected at Mace Head, Trinidad Head, Cape Matatula, Ragged Point, and Cape Grim and NOAA in situ measurements are made at Cape Matatula). Data from the two networks generally agree very well for this species with a mean bias (AGAGE minus NOAA) of around -0.02 pmol mol^{-1} and standard deviation of 0.05 pmol mol^{-1} (~1%) between coincident measurements (defined as being within 3 h of each other). This offset between the networks is consistent with measurements of air samples exchanged between NOAA-ESRL and SIO, for which a mean AGAGE minus NOAA difference of -0.02 ± 0.01 pmol mol^{-1} has also been derived. Where data from both networks are used in the inversions below, the NOAA-ESRL measurements were adjusted to the SIO-2005 scale by multiplication by a constant factor (0.998 ± 0.005) determined from comparison of coincident measurements.

3 Emissions inversion method

In order to use the measurements to estimate emission rates, an atmospheric chemical transport model is required, along with a suitable inverse method, and prior estimates of global SF_6 emissions. Here we outline these individual components of the inversion.

3.1 Atmospheric chemical transport model

The Model for Ozone and Related Tracers (MOZART v4.5, Emmons et al., 2009) was used to simulate three-dimensional SF_6 atmospheric mole fractions. The model has previously been demonstrated to accurately represent the variability and interhemispheric and vertical gradients of this species at NOAA sampling sites, assuming EDGAR emissions (Gloor et al., 2007). Meteorological data from the National Centers for Environmental Prediction/National Center for Atmospheric Research (NCEP/NCAR)

ACPD
10, 13519–13555, 2010

reanalysis project (Kalnay et al., 1996) were used to simulate the transport of SF_6, which was assumed to exhibit no chemical loss in the atmosphere or at the surface (i.e. an infinite lifetime was assumed).

We present two types of inversion in this paper, one estimating hemispheric emissions from 1970–2008 using the archived air samples and modern background measurements, and a second, from 2004–2008, in which continent-scale emissions were estimated, also incorporating non-background sites. NCEP/NCAR reanalyses were available for use with MOZART from 1990–2008 at 1.8°×1.8°resolution, with 28 vertical sigma levels extending from the surface to approximately 3 hPa. For reasons of computational efficiency, these dynamics data were interpolated to 5°latitude/longitude for the hemispheric 1970–2008 inversion, and monthly average background mole fractions were compared to the measurements. Since it is assumed that all the measurements represented background values in this part of the work, the resolution was not expected to significantly influence the derived emissions. Annually repeating 1990 dynamics was used between 1970 and 1990, and the error associated with this limitation was incorporated into our inverse estimates using the method described below. For the regional 2004–2008 inversion, we ran MOZART at 1.8°×1.8°resolution and output weekly average mole fractions.

3.2 Prior emissions

In both inversions, prior emissions estimates from EDGAR v4 (European Comission, 2009) were used and interpolated to the required grid resolution. These estimates currently exist only for 1970–2005, so we extrapolated the EDGAR values through the final years (2006–2008). The extrapolation was carried out by breaking the emissions field into separate continents and then subdividing continents into countries that report to the UNFCCC (these are the same regions used in the continental inversion). Emissions were then linearly projected in these regions using 2004 and 2005 EDGAR values. We estimated a 1-σ uncertainty in the inventory emissions of 10%, sequentially increasing to 20% between 2005 and 2008, since we expected that our simple

ACPD
10, 13519–13555, 2010

extrapolation of the EDGAR emissions was an increasingly poor approximation of the "true" emissions in later years. Global EDGAR v4 and projected emissions are shown in Fig. 2.

3.3 Sensitivity estimates and inverse method

Each inversion requires an estimate of the sensitivity of the atmospheric mole fractions at each measurement site to changes in emission rate from each region. A model reference run was performed using the EDGAR emissions. The emissions were then perturbed in each hemisphere/continental region uniformly throughout each year (c.f. Chen and Prinn, 2006). These "pulses" were tracked for two years and compared to the reference; one year during which the emissions were increased, and a further year where the emissions were returned to the reference value. After the second year the excess mole fraction due to the perturbation was similar at each station (in other words the excess SF_6 was almost fully mixed throughout the troposphere). For all subsequent times the perturbed mole fractions at each measurement site were assumed to tend exponentially towards the completely well mixed value with a timescale of one year (the inversions were not found to be sensitive to this mixing time, since most of the updates of the emissions occur within the first two years). The sensitivity to a change in emissions was then found by dividing the magnitude of these increases in mole fraction by the magnitude of the emissions perturbation.

A recursive Bayesian minimum variance (Kalman-type) filter was implemented to determine emissions using these sensitivities (Prinn, 2000). This technique provides an optimal estimate of the true emission rate by combining the prior estimates with the information provided by the measurements, with each weighted by their respective uncertainties. Using this method we show that the annual global emission rate can be constrained very well using the in situ measurements from the AGAGE and NOAA networks and the archived air samples, which together cover the period from 1973 to 2008. Regional emissions estimation for 2004–2008 were also obtained, but were more poorly constrained than the global values.

ACPD
10, 13519–13555, 2010

3.4 Measurement-model uncertainty estimation

The assumed total uncertainty on each monthly/weekly average mole fraction measurement included contributions from the measurements themselves, sampling frequency, model-data mismatch and a repeating dynamics uncertainty (where required):

$$\sigma^2 = \sigma^2_{\text{measurement}} + \sigma^2_{\text{sampling frequency}} + \sigma^2_{\text{mismatch}} + \sigma^2_{\text{dynamics}} \quad (1)$$

Here $\sigma_{\text{measurement}}$ is the estimated total uncertainty on each measurement, which includes measurement repeatability and scale propagation errors. Since we did not know the latter term exactly, we estimated it by comparisons of the co-located AGAGE and NOAA measurements. It was assumed to be equal to the unbiassed root-mean-square (RMS) difference between the networks (equal to around 1%). Where weekly or monthly average mole fractions were used, the repeatability error was reduced if multiple measurements were available. The reduction in this component was calculated as the square root of the number of days for which measurements were available in an averaging period. The one-day unit was chosen since this is the typical order of magnitude of the autocorrelation timescale of the data at the high-frequency sites, and is therefore a measure of how many "independent" estimates contributed to each (weekly/monthly) average mole fraction.

Since the high-frequency data provided a more representative estimate of a mole fraction averaged over some period, we also included a sampling frequency term ($\sigma_{\text{sampling frequency}}$) equal to the standard deviation of the variability divided by the square root of the number of measurements in that time period. This term was estimated at the archived and flask data points (for which no high-frequency data were available) from the standard deviation of the variability at the closest high-frequency measurements, scaled by the ratio of the flask and high-frequency mole fractions.

The transport model-data mismatch uncertainty, σ_{mismatch}, was estimated as the standard deviation of the difference between the model grid cell containing the measurement site and the eight surrounding grid cells (c.f. Chen and Prinn, 2006).

ACPD
10, 13519–13555, 2010

In the hemispheric 1970–2008 inversion, the use of annually repeating meteorology before 1990 was found to increase the uncertainty in the derived emissions by only a small amount, compared to the other terms in the Eq. 1. It affects two components of the inversion; the simulated mole fractions and the derived sensitivities. The magnitude of the first component (σ_{dynamics} in Eq. 1) was determined by running a one-year simulation multiple times with constant emissions, and identical initial conditions, but with different wind fields. This term was found to introduce a mean uncertainty of approximately 0.01 pmol mol^{-1} at the grid cells used, and was included in the inversion through Eq. 1. The influence of the choice of meteorological year in the derived sensitivities was investigated by running the inversion 1000 times with randomly perturbed sensitivities. The standard deviation of the random perturbations was again found by performing multiple runs for one year with different dynamics. This process introduced an uncertainty of approximately 1% of the global emissions in each hemisphere, and is added to the pre-1990 emissions uncertainty presented below.

The total estimated uncertainties are shown as error bars in Fig. 1 at the five background AGAGE stations.

4 Global and hemispheric emissions

We first estimated global and hemispheric emissions of SF_6 between 1970 and 2008 using the AGAGE measurements and inverse method outlined above. MOZART was run at 5°×5°using EDGAR v4 and extrapolated emissions to provide a prediction of atmospheric mole fractions and to estimate sensitivites of the mole fractions to hemispheric emissions changes. Monthly average modeled mole fractions were stored at each grid cell, to be compared to monthly averages of the measurements. To ensure that the modeled mole fractions were representative of background air, the values in the oceanic grid-cell "upwind" of the actual cell containing the measurements were used (i.e. we used the cell to the West of the coastal sites in the high latitudes, and to the East of the coastal tropical sites). This strategy was necessary, since at the

ACPD
10, 13519–13555, 2010

low resolution used, some of the cells containing a measurement site also contained a significant contribution from local land sources, thereby preventing the modeled mole fractions within the cell from simulating truly "background" values. For simplicity, we assume that all of the NH archive samples were taken at Trinidad Head (where the majority of the samples were collected), since the difference between background values at NH archive sites is typically much less than 0.1 pmol mol^{-1} (the typical magnitude of the total measurement-model uncertainty given by Eq. 1).

An initially well mixed atmosphere was assumed in 1970, thereby allowing three (model) years before the first measurement, to allow a reasonable inter-hemispheric and vertical profile to emerge. A longer spin-up period was not used since EDGAR v4 emissions begin in 1970. Therefore, a small error may be induced in the derived emissions in the first few years, due to an incomplete stratospheric profile being set up before the incorporation of the first measurement. The initial well-mixed mole fraction was solved for in the inversion.

The mole fractions predicted using MOZART with EDGAR v4 emissions were generally found to agree well with the observations (Fig. 1, upper panel), indicating that global EDGAR v4 estimates are reasonably reliable for at least the pre-2001 period. From 2001 onwards a growing discrepancy can be seen to emerge between the measurements and the model run with the EDGAR and extrapolated emissions, suggesting that emissions were somewhat underestimated.

Using the sensitivities estimated with the transport model, we derive a new estimate of emissions using EDGAR v4 as a prior. The estimated annual emissions are shown in Fig. 2 and are tabulated in Table 2. The global emission rate can be seen to grow steadily from below 1 Ggyr^{-1} in 1970 to 6.5 ± 0.5 Ggyr^{-1} in 1995. The emissions then drop to 5.0 ± 0.5 Ggyr^{-1} between 1996 and 2000 before increasing by 50 ± 25% from 2000 through 2008. The global emission rate of 7.5 ± 0.4 Ggyr^{-1} in 2008 is the highest in this record. Our estimates generally agree with the top-down estimates of Levin et al. (2010) (also shown in Fig. 2) who estimate a 6% error on their annual emissions. They also agree well with EDGAR v4 until around 2001. After 2001, the derived

ACPD
10, 13519–13555, 2010

emissions are significantly higher than the inventory, consistent with the discrepancy noted above between the prior modeled mole fractions and the measurements. Annual mean background mole fractions obtained by running MOZART with optimized emissions are given in Table 2.

A second hemispheric inversion was performed, incorporating several NOAA-ESRL background sites in addition to the AGAGE high-frequency and archive data (Table 1). These measurements begin from 1997, and therefore provide a slightly longer time series than the AGAGE in situ instruments. Several sites were not used, since their proximity to pollution sources, at the coarse model resolution used, made it difficult to identify nearby model grid cells that could be thought to represent background air. The emissions derived using both measurement networks are shown in Fig. 2 as a dotted line. The figure shows that the emissions derived using both networks do not deviate significantly from the AGAGE-only estimates in most years, adding confidence to our global estimates.

EDGAR places a higher percentage of emissions in the NH than previous estimates (for example the 94% estimate of Maiss and Levin, 1994), being between 96% and 100%, depending on the year. Our estimates do not deviate significantly from these values (Fig. 2, lower panel). However, it should be noted that some correlation exists between our hemispheric estimates (with an average R^2 of around 0.2). Therefore, whilst some hemispheric emissions information may be obtained from the measurements, one cannot be quite as confident in their value as one is in the global total. Between 2005 and 2008, our inversion indicates an increased weighting of the NH in the global total, showing that the increased emissions most likely originated predominantly from the NH.

The upper panel of Fig. 2 also shows the emissions reported by 39 countries to the UNFCCC, along with the EDGAR estimate of UNFCCC emissions. UNFCCC reports use a "bottom-up" methodology, and therefore have not incorporated any information from atmospheric data (it is unclear to what extent EDGAR consider atmospheric measurements in their SF_6 emissions estimates). Before 1995, Levin et al.

ACPD
10, 13519–13555, 2010

(2010) found that Japanese emissions were likely to be overestimated in the reported UNFCCC values, and we applied their correction to the 1990–1994 values here. UNFCCC emissions are substantially lower than the estimated global totals for all years. Whilst this is to be expected given that the reported emissions leave out many large emitters, the EDGAR estimates suggest that these countries may also be significantly under-reporting. Both sets of bottom-up estimates indicate that since 1995, the trend amongst UNFCCC countries has been to report dramatically reduced emissions. If this trend in the reports and in EDGAR are reliable, it therefore seems likely that the growth since 2000 has been mostly driven by non-UNFCCC reporting regions. In the next section we discuss the possibility of verifying these estimates using the atmospheric measurements.

5 Continental emissions estimation

We have identified a new surge in SF_6 emissions between 2000 and 2008, of a similar magnitude to that derived by Levin et al. (2010). For the last three years of this period there is not yet any inventory information available. Here we ask whether this increase can be attributed to specific regions using data from AGAGE and NOAA networks and the three-dimensional transport model.

The global emissions field was split into eight regions chosen to separate continents and UNFCCC reporting countries. The regions were: North America, South and Central America, Africa, European countries reporting to the UNFCCC, non-UNFCCC European countries, Asian UNFCCC countries, non-UNFCCC Asian countries and Oceania (Fig. 3). Therefore, only Asia and Europe are split into UNFCCC and non-UNFCCC regions as they are the only continents with significant emissions from both reporting and non-reporting countries (although non-reporting European countries represent a very small source). As above, the emissions in each of these regions was linearly extrapolated from 2006 to 2008 using the EDGAR 2004 and 2005 values, and uncertainties of 10% (2004 and 2005), increasing to 20% (2008) were assumed.

ACPD
10, 13519–13555, 2010

In addition to the five AGAGE measurement sites described above, additional AGAGE Medusa measurements from Jungfraujoch, Switzerland and Gosan, Korea were incorporated along with in situ and flask measurements from the NOAA network. NOAA flask data are collected at a frequency of approximately one pair of flasks per week at surface sites, and daily at tall tower sites, whilst the NOAA in situ measurements are approximately hourly. Sampling locations for the three networks are shown in Fig. 3 and coordinates and names of the sites given in Table 1.

MOZART was run at 1.8°×1.8°resolution for the period 2004–2008, using interannually varying meteorology. This period was chosen because AGAGE GC-MS Medusa measurements of SF_6 began in 2004. The model was used to estimate the sensitivity of weekly-average mole fractions to changes in annual emission rates from each of the regions. Weekly averages were used in order to extract emissions information from pollution events at the high-frequency measurement sites. In order to reproduce the flask measurements as accurately as possible, we compared the weekly minimum rather than the mean, to represent the conditional background sampling at these sites. Periods shorter than one week were not thought to be as well modeled at the coarse spatial resolution of the global model used. Further, for measurements averaged over timescales shorter than that of typical synoptic variability (about 1 week) the assumption of independent measurements, required in the inversion, may not be as valid.

Modeled mole fractions were output at the location of each AGAGE, NOAA flask and in situ station. However, it was found that significant biases existed between the modeled and measured mole fractions at some sites, which were difficult to explain through changes in emissions alone. In many instances, the bias could be reduced by moving the measurement location to an adjacent grid cell in the model. It therefore seems likely that some measurement locations shared model grid cells with significant local sources, which would then "pollute" the simulated measurements at all times. To correct this effect, the RMS difference between the model and the measurements was calculated at each grid cell in which the station truly resided, and at surrounding grid

ACPD
10, 13519–13555, 2010

cells, and a site was moved if a lower RMS error could be obtained by positioning the measurement in an adjacent grid cell. The error associated with the site location was investigated and included in our final error estimate (see below). The mole fractions predicted by the model with the a priori emissions estimates are shown in the auxiliary material.

Using the inversion technique described above, emissions from the regions were estimated in each year, using ~12 000 weekly-average measurements. The mole fractions obtained using the estimated emissions are shown in the auxiliary material. Significant error reduction was achieved in the inversion for emissions from the three major source regions: non-UNFCCC Asia, North America and UNFCCC-Europe, with little error reduction in the more minor emissions regions. However, highly significant correlations were obtained between the major regions (Fig. 4). In other words, the inversion was not able to fully resolve emissions from these areas.

The reason for the inability of the inversion to fully distinguish between different regions is thought to be two-fold. Firstly, most of the sites used here measure predominantly background air. Therefore, whilst the networks can constrain the global background very well, there is little influence of "polluted" air masses on the measurements, making it unclear which regions are responsible for any increase in the background. This is particularly true of the flask sites, where the sampling strategy generally attempts to avoid intercepting polluted air (i.e. air containing information on near-by emissions). The second problem may be one of low signal-to-noise. The effect of an increase in emissions in any one year in any region is to increase the hemispheric background, and to increase the size of pollution events (of, say, daily–weekly duration) at the monitoring sites close the source. A regional inversion therefore relies on being able to distinguish these "local" signals from the change in the global background that also results from the change. However, the typical size of these signals for this compound tends to be small compared to the measurement uncertainty at the existing monitoring sites (see auxiliary material, http://www.atmos-chem-phys-discuss.net/10/13519/2010/acpd-10-13519-2010-supplement.zip).

ACPD
10, 13519–13555, 2010

Given the large correlations found between the major emissions regions, it would be misleading to present regional annual emissions with uncertainties equal to the diagonal elements of the covariance matrix derived in the inversion, as this would assume that these quantities were independent. To estimate the uncertainty in a way that is sensitive to these spatial correlations, we used a method similar to the "bootstrap" (Efron, 1979), where the inversion was repeated 1000 times, each time with the measurement network randomly resampled. In each iteration, for each year of the inversion, a network with the same number of sites as in the original inversion was created by randomly selecting stations with replacement. In each iteration we also estimated the influence of short-range transport error, and of station placement (see above), on the derived emissions by randomly changing the location of each of the stations to one of the surrounding grid cells. This latter contribution to the total uncertainty was necessary despite our inclusion of a "mismatch" term in Eq. 1, since the uncertainties input to the minimum variance filter must be unbiased, and therefore probably do not fully account for the likely model-data mismatch. Further, as mentioned above, we opted here for a bootstrap uncertainty estimate, as opposed to presenting the covariance output by the filter, which would carry the terms in Eq. 1 through to the final uncertainty. The model-measurement uncertainty (Eq. 1) therefore serves mainly to provide a weighting of one site relative to another in this inversion. The annual regional emissions error was estimated from the distribution of the perturbed estimates obtained. Using this technique, we obtained uncertainties that measure the sensitivity of the inversion to the network configuration and the influence of short-range transport errors.

The derived emissions are shown in Fig. 5, and are tabulated in the auxiliary material. The figure shows that using our uncertainty estimates, the emissions are relatively poorly constrained. In fact for most regions, in most years, little significant deviation from the prior is found, and no significant trend can be inferred. The exception is for non-UNFCCC Asian emissions, which shows a large upward trend in emissions from $2.1^{2.4}_{1.7}\,\mathrm{Ggyr}^{-1}$ in 2004 to $4.2^{5.2}_{2.5}\,\mathrm{Ggyr}^{-1}$ in 2008. This rise would account for all of the required global emissions growth between 2004 and 2008 ($1.8 \pm 0.5\,\mathrm{Ggyr}^{-1}$). Our

ACPD
10, 13519–13555, 2010

inversion also indicates that European emissions may be overestimated in EDGAR for 2004 and 2005. When compared to the UNFCCC estimates, we find it likely that the reported global SF_6 emissions are under-reported: The sum of the lower uncertainty limits for the emissions derived from UNFCCC reporting regions are 2.5, 2.2, 1.9, 2.0 $Ggyr^{-1}$ from 2004 to 2007 respectively (2007 is the latest year for which reports are currently available), compared to the 1.6, 1.5, 1.6, 1.5 $Ggyr^{-1}$ reported global totals.

There are few regional "top-down" emissions estimates currently available, that cover similar spatial scales, with which we can compare our estimates. Using airborne measurements, a Lagrangian transport model, carbon monoxide (CO) versus SF_6 ratios and a CO inventory, Hurst et al. (2006) found that North American emissions were 0.6 ± 0.2 $Ggyr^{-1}$ in 2003, compared to approximately $1.4^{2.0}_{1.2}$ $Ggyr^{-1}$ averaged over the period of our work. Whilst our values are roughly consistent with EDGAR v4, the Hurst et al. (2006) estimates are consistent with emissions reported to the UNFCCC. The reasons for this apparent discrepancy are unclear. Potential sources of error could include biases in either transport model used, a bias in the EDGAR prior influencing our derived emissions, or unaccounted for errors in the CO inventory influencing their estimates. These differences, and indeed differences between UNFCCC reports and EDGAR estimates highlight the need for improved regional emissions estimation in future.

In order for regional emissions validation to become more accurate for this species, more information is required in the inversion. This may be achievable in a number of ways. Firstly, the addition of many more high-frequency monitoring sites in regions that regularly intercept non-background air should increase the number of regions that could be distinguished. Secondly, the use of higher resolution transport models in regions close to high-frequency monitoring sites may allow us to extract a higher information content from the existing stations. For example, weekly averages were used here since we did not have confidence that the global model would be able to resolve shorter timescales. Further, the coarse resolution of current global models means that

ACPD
10, 13519–13555, 2010

local sources will not be well resolved at stations which are relatively close to polluted regions (e.g. Gosan, Korea, or Mace Head, Ireland). Therefore, it may be possible to extract more information from the higher-frequency (hourly-daily) measurements, potentially with a higher signal-to-noise ratio (since the smoothing effect of averaging can be avoided), provided the appropriate model is used.

6 Conclusions

We have presented new atmospheric SF_6 mole fraction measurements from the 1970s to 2008 in both hemispheres, comprising archived air samples and modern high-frequency data from the AGAGE network. Global emissions of this potent greenhouse gas were obtained using the AGAGE data alone and AGAGE plus NOAA-ESRL data, with a three-dimensional chemical transport model and an inverse method. These emissions were generally found to compare well with EDGAR v4 between 1970 and 2005 (the period for which inventory data currently exists). Since 2000, emissions have increased dramatically, and are now higher than at any point in the period investigated, reaching $7.5 \pm 0.4\,\mathrm{Gg\,yr^{-1}}$ in 2008. The global-average growth rate for 2008 was found to be $0.29 \pm 0.02\,\mathrm{pmol\,mol^{-1}\,yr^{-1}}$.

Regional emissions estimates were obtained for the period 2004–2008 using AGAGE and NOAA measurements. Significant correlations were found between the emissions derived in the inversion for the three major centers (North America, Europe, non-UNFCCC Asia). However, it was found that much of the emissions growth between 2004 and 2008 could most likely be attributed to non-UNFCCC Asian countries. No significant trends could be derived from the other emissions regions given the very large uncertainties obtained in the inversion. However, even with these large uncertainties, we find it likely that the emissions reported to the UNFCCC were underestimated between 2004 and 2007.

ACPD
10, 13519–13555, 2010

Acknowledgements. The AGAGE research program is supported by the NASA Upper Atmospheric Research Program in the US with grants NNX07AE89G to MIT, NNX07AF09G and NNX07AE87G to SIO, Defra and NOAA in the UK, CSIRO and the Australian Government Bureau of Meteorology in Australia. We wish to thank Louisa Emmons and Stacy Walters at NCAR for their invaluable help on the use of the MOZART v4 model. We especially thank S. A. Montzka (NOAA/GMD), C. D. Keeling (deceased) and R. F. Keeling (SIO), and R. C. Rhew (UCB) for air samples. We also thank R. A. Rasmussen and the Oregon Graduate Institute (OGI) for originally collecting the Cape Meares Northern Hemispheric samples which were provided by NOAA-ESRL, NILU, and CSIRO. We are grateful to Marc Fisher at the Lawrence Berkeley National Laboratory for operating the WCG and STR tower sites with support from the California Energy Commission's Public Interest Environmental Research program. We are also grateful to Arlyn Andews for her contributions regarding the NOAA tower measurements. We thank Ingeborg Levin, University of Heidelberg, for providing SF_6 data shown in the auxiliary material. We are extremely grateful to Nada Derek (CSIRO) for her valuable work in compiling UNFCCC emissions estimates for use in this paper. We are indebted to the staff at the AGAGE and NOAA sites for their continuing contributions to produce high quality measurements of atmospheric trace gases. In particular, we are indebted to the late Laurie Porter, whose meticulous work and incisive mind contributed so much to the SF_6 record from Cape Grim.

References

Busenberg, E. and L. N. Plummer: Dating Young Groundwater with Sulfur Hexafluoride: Natural and Anthropogenic Sources of Sulfur Hexafluoride, Water Resour. Res., 36(10), 3011–3030, doi:10.1029/2000WR900151, 2000. 13523

Chen, Y.-H. and Prinn, R. G.: Estimation of atmospheric methane emissions between 1996 and 2001 using a three-dimensional global chemical transport model, J. Geophys. Res.-Atmos., 111, D10307, doi:10.1029/2005JD006058, 2006. 13531, 13532

European Comission: Joint Research Centre (JRC)/Netherlands Environmental Assessment Agency (PBL), Emission Database for Global Atmospheric Research (EDGAR), release version 4.0, http://edgar.jrc.ec.europa.eu, 2009. 13524, 13530

Deeds, D. A., Vollmer, M. K., Kulongoski, J. T., Miller, B. R., Mühle, J., Harth, C. M., Izbicki, J. A., Hilton, D. R., and Weiss, R. F.: Evidence for crustal degassing of SF_6

ACPD

10, 13519–13555, 2010

and SF_6 in Mojave Desert groundwaters, Geochim. Cosmochim. Ac. , 72, 999–1013, doi:10.1016/j.gca.2007.11.027, 2008. 13522
Dlugokencky, E., Steele, L. P., Lang, P., and Masarie, K.: The growth rate and distribution of atmospheric methane, J. Geophys. Res., 99, 17021–17043, 1994. 13527
Efron, B.: 1977 Rietz Lecture – Bootstrap Methods – Another look at the jackknife, Ann. Stat., 7, 1–26, 1979. 13539
Elkins, J. W. and Dutton, G. S.: Nitrous oxide and sulfur hexafluoride, [in State of the Climate in 2008], Bull. Amer. Meteor. Soc., 90(8), S1–S196, 2009. 13527
Emmons, L. K., Walters, S., Hess, P. G., Lamarque, J.-F., Pfister, G. G., Fillmore, D., Granier, C., Guenther, A., Kinnison, D., Laepple, T., Orlando, J., Tie, X., Tyndall, G., Wiedinmyer, C., Baughcum, S. L., and Kloster, S.: Description and evaluation of the Model for Ozone and Related chemical Tracers, version 4 (MOZART-4), Geosci. Model Dev., 3, 43–67, doi:10.5194/gmd-3-43-2010, 2010. 13529
Forster, P., Ramaswamy, V., Artaxo, P., Berntsen, T., Betts, R., Fahey, D. W., Haywood, J., Lean, J., Lowe, D. C., Myhre, G., Nganga, J., Prinn, R., Raga, G., Schulz, M., and Van Dorland, R.: Changes in Atmospheric Constituents and in Radiative Forcing, in: Climate Change 2007: The Physical Science Basis. Contribution of Working Group I to the Fourth Assessment Report of the Intergovernmental Panel on Climate Change, edited by: Solomon, S., Qin, D., Manning, M., Chen, Z., Marquis, M., Averyt, K. B., Tignor, M., and Miller, H. L., Cambridge University Press, Cambridge, United Kingdom and New York, NY, USA, 2007. 13522
Fraser, P. J., Porter, L. W., Baly, S. B., Krummel, P. B., Dunse, B. L., Steele, L. P., Derek, N., Langenfelds, R. L., Levin, I., Oram, D. E., Elkins, J. W., Vollmer, M. K., and Weiss, R. F.: Sulfur hexafluoride at Cape Grim: long term trends and regional emissions, in: Baseline Atmospheric Program Australia 2001-2002, edited by: Cainey, J. M., Derek, N., and Krummel, P. B., Bureau of Meteorology and CSIRO Atmospheric Research, 18–23, 2004. 13522, 13523, 13524
Geller, L., Elkins, J. W., Lobert, J., Clarke, A., Hurst, D. F., Butler, J., and Myers, R.: Tropospheric SF_6: Observed latitudinal distribution and trends, derived emissions and interhemispheric exchange time, Geophys. Res. Lett., 24, 675–678, 1997. 13522, 13528
Gloor, M., Dlugokencky, E., Brenninkmeijer, C., Horowitz, L., Hurst, D. F., Dutton, G., Crevoisier, C., Machida, T., and Tans, P.: Three-dimensional SF_6 data and tropospheric transport simulations: Signals, modeling accuracy, and implications for inverse modeling, J. Geophys.

ACPD
10, 13519–13555, 2010

Res.-Atmos., 112, D15112, doi:10.1029/2006JD007973, 2007. 13523, 13529
Hall, T. and Waugh, D.: Tracer transport in the tropical stratosphere due to vertical diffusion and horizontal mixing, Geophys. Res. Lett., 24, 1383–1386, 1997. 13523
Hurst, D. F., Lin, J. C., Romashkin, P. A., Daube, B. C., Gerbig, C. , Matross, D. M., Wofsy, S. C., Hall, B. D., and Elkins, J. W.: Continuing global significance of emissions of Montreal Protocol restricted halocarbons in the United States and Canada, J. Geophys. Res., 111, D15302, doi:10.1029/2005JD006785, 2006. 13523, 13540
Kalnay, E., Kanamitsu, M., Kistler, R., Collins, W., Deaven, D., Gandin, L., Iredell, M., Saha, S., White, G., Woollen, J., Zhu, Y., Chelliah, M., Ebisuzaki, W., Higgins, W., Janowiak, J., Mo, K., Ropelewski, C., Wang, J., Leetmaa, A., Reynolds, R., Jenne, R., and Joseph, D.: The NCEP/NCAR 40-year reanalysis project, B. Am. Meteorol. Soc., 77, 437–471, 1996. 13530
Langenfelds, R. L., Fraser, P. J., Francey, R. J., Steele, L. P., Porter, L. W., and Allison, C. E.: The Cape Grim air archive: The first seventeen years, 1978–1995, in: Baseline Atmospheric Program (Australia) 1994–95, edited by: Francey, R. J., Dick, A. L., and Derek, N., pp. 53–70, 1996. 13525, 13526
Levin, I., Naegler, T., Heinz, R., Osusko, D., Cuevas, E., Engel, A., Ilmberger, J., Langenfelds, R. L., Neininger, B., Rohden, C. v., Steele, L. P., Weller, R., Worthy, D. E., and Zimov, S. A.: The global SF6 source inferred from long-term high precision atmospheric measurements and its comparison with emission inventories, Atmos. Chem. Phys., 10, 2655–2662, doi:10.5194/acp-10-2655-2010, 2010. 13523, 13524, 13526, 13527, 13534, 13535, 13536, 13552
Maiss, M. and Levin, I.: Global Increase Of SF_6 Observed In The Atmosphere, Geophys. Res. Lett., 21, 569–572, 1994. 13522, 13535
Maiss, M., Steele, L., Francey, R., Fraser, P., Langenfelds, R., Trivett, N., and Levin, I.: Sulfur hexafluoride – A powerful new atmospheric tracer, Atmos. Environ., 30(10–11), 1621–1629, 1996. 13522, 13526, 13527
Miller, B. R., Weiss, R. F., Salameh, P. K., Tanhua, T., Greally, B. R., Mühle, J., and Simmonds, P. G.: Medusa: A sample preconcentration and GC/MS detector system for in situ measurements of atmospheric trace halocarbons, hydrocarbons, and sulfur compounds, Anal. Chem., 80, 1536–1545, doi:10.1021/ac702084k, 2008. 13524, 13526
Niemeyer, L. and Chu, F.: SF_6 and the Atmosphere, IEEE. T. Electr. Insul., 27(1), 184–187, 1992. 13522
Patra, P. K., Takigawa, M., Dutton, G. S., Uhse, K., Ishijima, K., Lintner, B. R., Miyazaki, K., and

ACPD
10, 13519–13555, 2010

Elkins, J. W.: Transport mechanisms for synoptic, seasonal and interannual SF_6 variations and "age" of air in troposphere, Atmos. Chem. Phys., 9, 1209–1225, doi:10.5194/acp-9-1209-2009, 2009. 13523

Peters, W., Krol, M., Dlugokencky, E., Dentener, F., Bergamaschi, P., Dutton, G., von Velthoven, P., Miller, J., Bruhwiler, L., and Tans, P.: Toward regional-scale modeling using the two-way nested global model TM5: Characterization of transport using SF_6, J. Geophys. Res.-Atmos., 109, doi:10.1029/2004JD005020, 2004. 13523

Prinn, R.: Measurement Equation for Trace Chemicals in Fluids and Solution of its Inverse, in: Inverse Methods in Global Biogeochemical Cycles, edited by: Kasibhatla, P., Heimann, M., Mahowald, N., Prinn, R. G., and Hartley, D. E., American Geophysical Union, Washington DC, 2000. 13531

Prinn, R., Weiss, R., Fraser, P., Simmonds, P., Cunnold, D., Alyea, F., O'Doherty, S., Salameh, P., Miller, B., Huang, J., Wang, R., Hartley, D., Harth, C., Steele, L., Sturrock, G., Midgley, P., and McCulloch, A.: A history of chemically and radiatively important gases in air deduced from ALE/GAGE/AGAGE, J. Geophys. Res., 105(D14), 17751–17792, doi:10.1029/2000JD900141, 2000. 13523, 13527

Ravishankara, A., Solomon, S., Turnipseed, A., and Warren, R.: Atmospheric Lifetimes of Long-Lived Halogenated Species, Science, 259, 194–199, 1993. 13522

Rinsland, C., Brown, L., and Farmer, C.: Infrared Spectroscopic Detection of Sulfur-Hexafluoride (SF_6) in the Lower Stratosphere and Upper Troposphere, J. Geophys. Res.-Atmos., 95, 5577–5585, 1990. 13522

Santella, N., Ho, D. T., Schlosser, P., and Stute, M.: Widespread elevated atmospheric SF_6 mixing ratios in the Northeastern United States: Implications for groundwater dating, J. Hydrol., 349, 139–146, doi:10.1016/j.jhydrol.2007.10.031, 2008.

UNFCCC: United Nations Framework Convention on Climate Change, National Inventory Submissions 2010, http://unfccc.int/national_reports/annex_i_ghg_inventories/national_inventories_submissions/items/5270.php, 2010. 13524

Vollmer, M. K. and Weiss, R. F.: Simultaneous determination of sulfur hexafluoride and three chlorofluorocarbons in water and air, Mar. Chem., 78, 137–148, 2002. 13522

Vollmer, M. K., Zhou, L. X., Greally, B. R., Henne, S., Yao, B., Reimann, S., Stordal, F., Cunnold, D. M., Zhang, X. C., Maione, M., Zhang, F., Huang, J., and Simmonds, P. G.: Emissions of ozone-depleting halocarbons from China, Geophys. Res. Lett., 36, doi:10.1029/2009GL038659, 2009. 13523

ACPD
10, 13519–13555, 2010

Table 1. Site identification codes, names and locations. An asterisk (*) in the first column denotes a site used in the AGAGE-only global inversion, and a plus (+) denotes a site used in the AGAGE-NOAA global inversion. All sites are used in the regional inversion.

Code	Name	Network	Site type	Lat. (°N)	Lon. (°E)	Alt. (m a.s.l.)
ALT^{+}	Alert, Nunavut	NOAA	Flask	82.4	297.5	200
ASC^{+}	Ascension Island	NOAA	Flask	−7.9	345.6	54
ASK	Assekrem	NOAA	Flask	23.2	5.4	2728
AZR	Terceira Island, Azores	NOAA	Flask	38.8	332.6	40
BAL	Baltic Sea	NOAA	Flask	55.3	17.2	3
BAO	Boulder Atmospheric Observatory, Colorado	NOAA	Tower	40.0	255.0	1584
BKT	Bukit Kototabang	NOAA	Flask	−0.2	100.3	864
BME	St. Davids Head, Bermuda	NOAA	Flask	32.4	295.4	30
BMW^{+}	Tudor Hill, Bermuda	NOAA	Flask	32.3	295.1	30
BRW^{+}	Barrow, Alaska	NOAA	In situ	71.3	203.4	11
BSC	Black Sea, Constanta	NOAA	Flask	44.2	28.7	3
CBA	Cold Bay, Alaska	NOAA	Flask	55.2	197.3	21
CGO^{*+}	Cape Grim, Tasmania	AGAGE NOAA	In situ, flask	−40.4	144.6	104
CHR	Christmas Island	NOAA	Flask	1.7	202.8	3
CRZ	Crozet Island	NOAA	Flask	−46.5	51.8	120
EIC^{+}	Easter Island	NOAA	Flask	−27.1	250.6	50
GMI	Mariana Islands	NOAA	Flask	13.4	144.8	1
GSN	Gosan, Korea	AGAGE	In situ	33.3	126.2	47
HBA^{+}	Halley Station, Antarctica	NOAA	Flask	−75.6	333.5	30
HUN	Hegyhatsal	NOAA	Flask	47.0	16.6	248
ICE^{+}	Storhofdi, Vestmannaeyjar	NOAA	Flask	63.4	339.7	118

ACPD
10, 13519–13555, 2010

Table 1. Continued.

Code	Name	Network	Site type	Lat. (°N)	Lon. (°E)	Alt. (m a.s.l.)
IZO[+]	Tenerife, Canary Islands	NOAA	Flask	28.3	343.5	2360
JFJ	Jungfraujoch, Switzerland	AGAGE	In situ	46.5	8.0	3580
KEY	Key Biscayne, Florida	NOAA	Flask	25.7	279.8	3
KUM	Cape Kumukahi, Hawaii	NOAA	Flask	19.5	205.2	3
KZD	Sary Taukum	NOAA	Flask	44.1	76.9	601
KZM	Plateau Assy	NOAA	Flask	43.2	77.9	2519
LEF	Park Falls, Wisconsin	NOAA	Flask	46.0	269.7	472
MHD[*+]	Mace Head, Ireland	AGAGE NOAA	In situ, flask	53.3	350.1	25
MID[+]	Sand Island, Midway	NOAA	Flask	28.2	182.6	3
MLO[+]	Mauna Loa, Hawaii	NOAA	In situ	19.5	204.4	3397
NWR	Niwot Ridge, Colorado	NOAA	In situ	40.0	254.4	3025
NWR	Niwot Ridge, Colorado	NOAA	Flask	40.0	254.4	3523
PAL	Pallas-Sammaltunturi, GAW Station	NOAA	Flask	68.0	24.1	560
POC	Pacific Ocean Cruise	NOAA	Flask	–	–	–
PSA[+]	Palmer Station, Antarctica	NOAA	Flask	−64.9	296.0	10
RPB[*+]	Ragged Point, Barbados	AGAGE NOAA	In situ, flask	13.2	301.0	42
SEY[+]	Mahe Island	NOAA	Flask	−4.7	55.2	3
SHM	Shemya Island, Alaska	NOAA	Flask	52.7	174.1	40
SMO[*+]	Cape Matatula, Samoa	AGAGE NOAA	In situ, flask	−14.2	189.4	77
SPO[+]	South Pole, Antarctica	NOAA	In situ	−90.0	335.2	2810
STM	Ocean Station M	NOAA	Flask	66.0	2.0	0

ACPD
10, 13519–13555, 2010

Table 1. Continued.

Code	Name	Network	Site type	Lat. (°N)	Lon. (°E)	Alt. (m a.s.l.)
STR[a]	Sutro Tower, San Francisco, California	NOAA	Tower	37.8	237.6	254
SUM[+]	Summit	NOAA	In situ, flask	72.6	321.5	3238
SYO[+]	Syowa Station, Antarctica	NOAA	Flask	−69.0	39.6	11
TAP	Tae-ahn Peninsula	NOAA	Flask	36.7	126.1	20
TDF	Tierra Del Fuego, Ushuaia	NOAA	Flask	−54.9	291.5	20
THD[*+]	Trinidad Head, California	AGAGE NOAA	In situ, flask	41.1	235.9	140
UTA	Wendover, Utah	NOAA	Flask	39.9	246.3	1320
UUM	Ulaan Uul	NOAA	Flask	44.5	111.1	914
WBI	West Branch, Iowa	NOAA	Tower	41.7	268.6	241
WGC[a]	Walnut Grove, California	NOAA	Tower	38.3	238.5	0
WIS	Sede Boker, Negev Desert	NOAA	Flask	31.1	34.9	400
WKT	Moody, Texas	NOAA	Tower	31.3	262.7	251
WLG	Mt. Waliguan	NOAA	Flask	36.3	100.9	3810
ZEP[+]	Ny Alesund, Svalbard	NOAA	Flask	78.9	11.9	474

[a] Air samples at these sites were collected in collaboration between NOAA and the US Department of Energy, Environmental Energy Technologies Division at Lawrence Berkeley National Laboratory

ACPD
10, 13519–13555, 2010

Table 2. Annual optimized emissions and associated errors, and surface background mole fractions in each semi-hemisphere, 1973–2008. Mole fractions are output from MOZART run with optimized emissions. Background values are defined as the median mole fraction of oceanic grid cells at the lowest model level.

Year	Emissions ($Ggyr^{-1}$)	Error ($Ggyr^{-1}$)	Surface background mole fraction ($pmolmol^{-1}$)			
			30°N–90°N	0°N–30°N	30°S–0°S	90°S–30°S
1970	0.73	0.08	0.29	0.28	0.27	0.27
1971	0.85	0.09	0.34	0.32	0.29	0.29
1972	0.91	0.10	0.37	0.35	0.33	0.32
1973	1.06	0.12	0.41	0.39	0.36	0.36
1974	1.11	0.12	0.46	0.44	0.40	0.40
1975	1.33	0.14	0.51	0.49	0.45	0.44
1976	1.59	0.17	0.57	0.55	0.50	0.49
1977	1.79	0.19	0.65	0.62	0.56	0.55
1978	1.98	0.21	0.73	0.69	0.63	0.62
1979	2.39	0.24	0.82	0.78	0.71	0.70
1980	2.57	0.26	0.92	0.88	0.81	0.79
1981	2.74	0.27	1.03	0.99	0.91	0.89
1982	2.99	0.29	1.15	1.10	1.01	1.00
1983	3.08	0.30	1.28	1.22	1.13	1.11
1984	3.52	0.34	1.42	1.36	1.25	1.23
1985	3.88	0.37	1.57	1.51	1.39	1.37
1986	4.16	0.39	1.74	1.67	1.54	1.52
1987	4.34	0.40	1.92	1.84	1.70	1.68
1988	4.54	0.41	2.10	2.01	1.87	1.84
1989	4.91	0.46	2.31	2.20	2.05	2.02

ACPD
10, 13519–13555, 2010

Table 2. Continued.

Year	Emissions ($Ggyr^{-1}$)	Error ($Ggyr^{-1}$)	Surface background mole fraction ($pmolmol^{-1}$)			
			30°N–90°N	0°N–30°N	30°S–0°S	90°S–30°S
1990	5.04	0.47	2.51	2.40	2.24	2.20
1991	5.27	0.52	2.72	2.60	2.43	2.40
1992	5.44	0.54	2.93	2.81	2.64	2.60
1993	5.70	0.53	3.17	3.03	2.85	2.81
1994	5.99	0.53	3.41	3.26	3.07	3.03
1995	6.49	0.53	3.67	3.51	3.30	3.26
1996	6.13	0.54	3.92	3.75	3.55	3.50
1997	6.01	0.48	4.14	3.98	3.79	3.75
1998	5.41	0.49	4.32	4.21	4.02	3.98
1999	5.13	0.47	4.52	4.39	4.23	4.19
2000	4.99	0.46	4.70	4.58	4.43	4.40
2001	5.01	0.44	4.88	4.77	4.63	4.59
2002	5.56	0.43	5.09	4.99	4.83	4.79
2003	6.19	0.39	5.35	5.23	5.04	5.01
2004	5.71	0.36	5.56	5.46	5.28	5.24
2005	6.35	0.34	5.80	5.69	5.50	5.47
2006	6.47	0.34	6.06	5.94	5.75	5.71
2007	7.17	0.36	6.34	6.22	6.01	5.96
2008	7.54	0.44	6.65	6.51	6.29	6.24

ACPD
10, 13519–13555, 2010

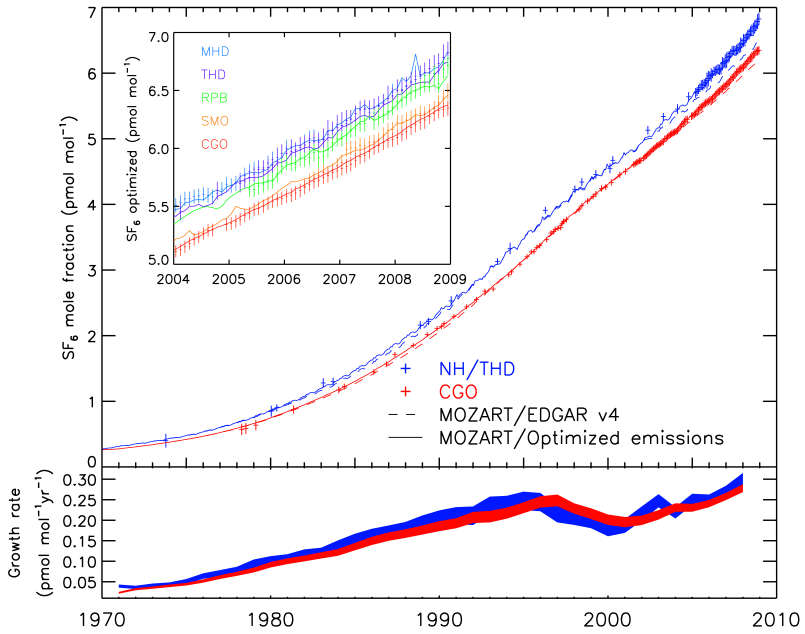

Fig. 1. AGAGE archived air and in situ measurements at Cape Grim, Tasmania (red) and NH sites (mostly Trinidad Head and La Jolla, CA, blue). The dashed lines show the atmospheric mole fraction predicted by MOZART using EDGAR v4 emissions (extrapolated for 2006–2008), and the solid lines show the mole fraction computed using the optimally-estimated emissions. Error bars on the measurements include sampling and modeling uncertainty, as shown in Eq. 1. The inlay in the upper panel shows the measured mole fractions at the five background AGAGE sites used in the global inversion and modeled mole fractions using the optimally-estimated emissions. The lower panel shows the optimized growth rate at Cape Grim and the NH sites, with the line thickness denoting the 1-σ uncertainty.

ACPD
10, 13519–13555, 2010

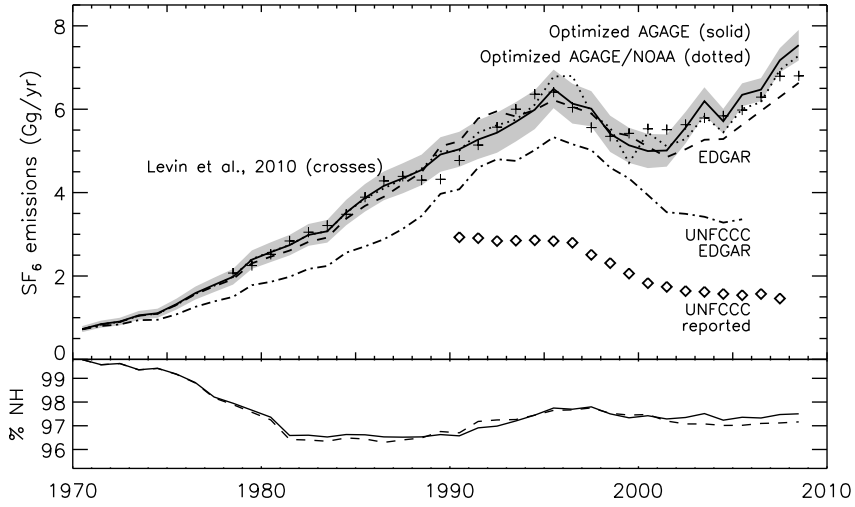

Fig. 2. Optimized global SF_6 emissions derived using AGAGE data only (solid line) and AGAGE and NOAA-ESRL data (dotted line). EDGAR v4 emissions are shown as a dashed line, with UNFCCC-reported emissions as diamonds, and EDGAR v4 estimates of UNFCCC emissions as the dash-dotted line. Shaded areas show the 1-σ uncertainties in the optimized AGAGE-only emissions. Levin et al. (2010) top-down emissions are shown as crosses. UNFCCC reported emissions have been adjusted prior to 1995 as per Levin et al. (2010). The lower panel shows the percentage emission in the NH, according to our AGAGE-only inversion (solid) and EDGAR v4 (dashed).

ACPD
10, 13519–13555, 2010

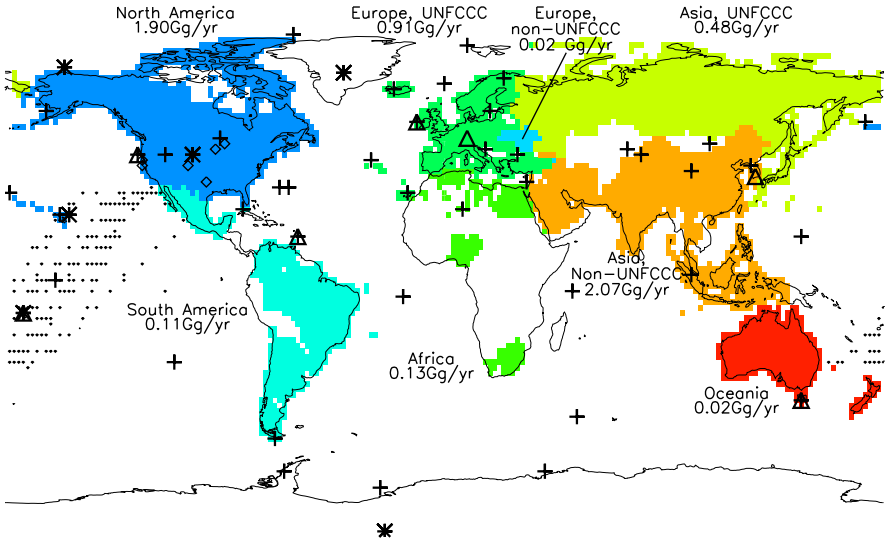

Fig. 3. Eight regions whose emissions were estimated in our regional inversion. Colored areas show grid cells (1.8°×1.8°resolution) where EDGAR predicts non-zero emissions. Measurement locations are shown for AGAGE (triangles), NOAA in situ (asterisks), tower (diamonds), surface flask sites (crosses) and NOAA Pacific Ocean Cruise tracks (dots). The site location shown here refers to the assumed position within the model and may differ from the true location as outlined in the text. The quoted emissions are the regional EDGAR v4 estimates for 2005.

ACPD
10, 13519–13555, 2010

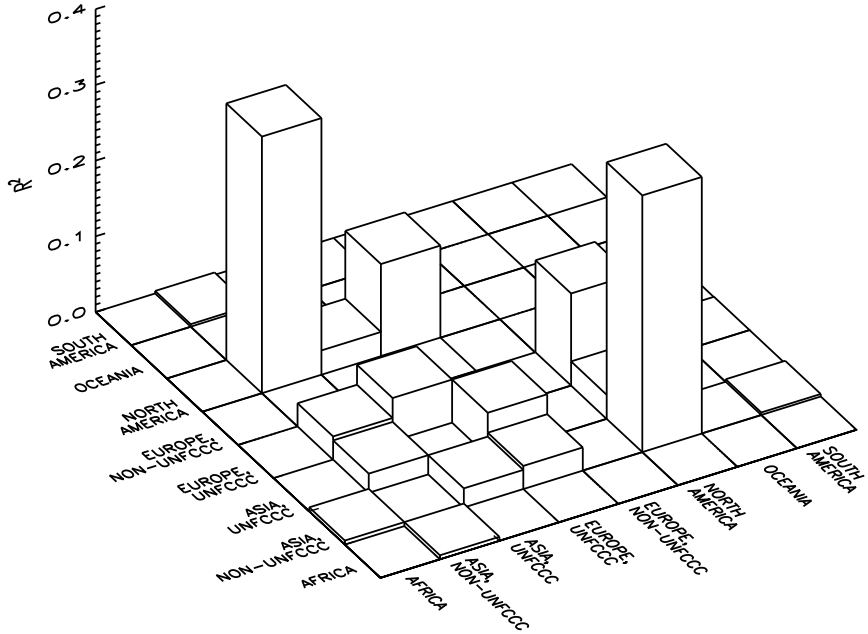

Fig. 4. Average correlations (R^2) between optimized emissions from the eight regions, 2004–2008. Diagonal elements (identically equal to 1) are set to zero for clarity.

ACPD
10, 13519–13555, 2010

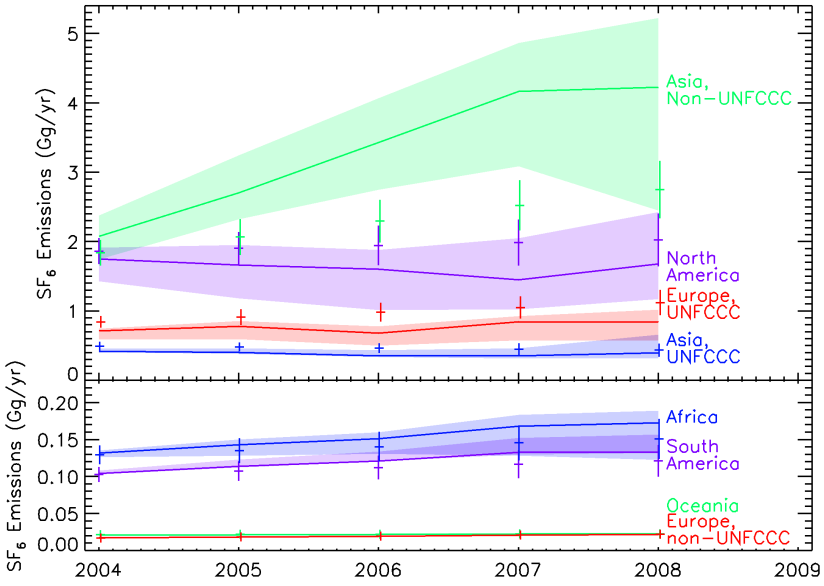

Fig. 5. Regional SF_6 emission rates and 68% uncertainty range (shaded areas). Uncertainties are estimated using the bootstrap technique outlined in the text. The upper panel shows the four largest emitters, and the lower panel shows the smaller emissions regions. Crosses show the prior emissions estimates, with the size of the vertical line denoting the 1-σ assumed uncertainty.

ACPD
10, 13519–13555, 2010